I&EC research
Industrial & Engineering Chemistry Research

pubs.acs.org/IECR
Article

Air-Gap Membrane Distillation of Industrial Brine: Effect of Brine Concentration and Temperature

Patricia Ugarte, Simona Renda, Miguel Cano, Jorge Pérez, José Ángel Peña, and Miguel Menéndez*

Cite This: *Ind. Eng. Chem. Res.* 2024, 63, 1546−1553

ABSTRACT: Precipitated silica is a highly required and employed product on the worldwide market; its production involves the reaction of sulfuric acid and sodium silicate in aqueous solutions, leading to the undesired generation of a significant volume of brine containing Na_2SO_4. The treatment of this brine is crucial within the framework of a circular economy, as it enables the dual objective of preventing pollution and extracting value from waste. This study focused, at first, on evaluating the performances of the air-gap membrane distillation (AGMD) technology using a synthetic Na_2SO_4 brine. Then, the feasibility of applying this technology to the concentration of an industrial Na_2SO_4 brine was evaluated. To achieve these goals, an AGMD pilot plant with a flat sheet membrane module with an effective area of 0.025 m^2 was employed. The effects of the brine concentration and feed temperature on flux were analyzed. It was observed that the flow rate and the temperature of the brine were significant parameters influencing the magnitude of the permeate flux, while flow rate and temperature of the cooling water were not particularly influential. The industrial brine concentration ranged from 120 to 270 g/L, and continuous 2-month operation was successfully achieved. Very low values for permeate conductivity were observed (1−12 μS/cm), and values close to 100% for salt rejection were measured, resulting in perfectly depurated water. A 1-D model for flat sheet-type AGMD was also developed, and it was observed to strongly correlate with the experimental data. Since no adjustable parameters were included in the model, this result validates the experimental tests and suggests that the model could be further employed to predict with accuracy many different operating conditions.

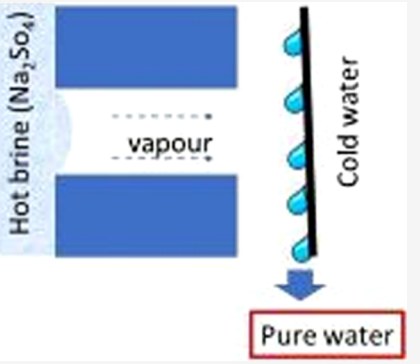

INTRODUCTION

Precipitated silica is a widely employed material, with a global market larger than 4 billion euros and applications in many industries, like rubber, painting, food, or pharma.[1] It is produced by neutralizing sodium silicate with sulfuric acid,[2] with a reaction (eq 1) that generates as a byproduct a high conductivity salt stream. The salt generated in the process, sodium sulfate (Na_2SO_4), must be removed from silica by washing, thus determining huge water consumption. The waste of the separation process, constituted of a Na_2SO_4 aqueous solution, is conventionally addressed as brine.

$$r{\cdot}SiO_2{\cdot}Na_2O + H_2SO_4 \rightarrow r{\cdot}SiO_2 + Na_2SO_4 + H_2O \quad (1)$$

Within the context of circular economy, the concept of zero liquid discharge must be applied to reduce brine release, minimize water consumption, and recover sodium sulfate as a valuable product. Given the dimension of precipitated silica market, the sustainable disposal of the Na_2SO_4 brine is becoming an issue of emerging interest. The application of novel technologies to this process is highly captivating for the chemical industry, where research for more sustainable solutions must align with the economic viability of a process. The conventional method for brine treatment is represented by reverse osmosis (RO), which is a process suitable for low salt concentration since high salinity requires a high osmotic pressure.[3] This sets a limit to the concentration of the brine that can be reached by RO and leads to a more concentrated brine that cannot be treated any further. To handle highly concentrated solutions, membrane distillation (MD)[4] represents a cutting-edge technology, a process that can be conducted with different configurations, giving rise to several types of MD: direct contact membrane distillation (DCMD), air-gap membrane distillation (AGMD), swept gas membrane distillation and vacuum membrane distillation.[5]

The MD process involves a phase change from liquid to vapor on one side of the membrane and condensation from vapor to liquid on the other. In MD, a hydrophobic porous membrane is employed to allow water vapor to pass through its pores. Moreover, as only water vapor can pass through the membrane, a salt rejection of almost 100% is achieved. Unlike

Received: September 27, 2023
Revised: December 15, 2023
Accepted: December 22, 2023
Published: January 9, 2024

https://doi.org/10.1021/acs.iecr.3c03415
Ind. Eng. Chem. Res. 2024, 63, 1546−1553

the RO, MD does not require a high hydraulic pressure for mass transfer. Therefore, MD is a very promising technology for the treatment of highly saline solutions.[6−9]

The main advantages of MD technology compared to other separation processes can be summed up as follows: (1) low operating temperatures (<80 °C) which allows the use of low quality energy (industrial waste heat or solar energy);[10−13] (2) MD works at atmospheric pressure which decreases fouling and pore plugging, unlike RO; (3) the feed usually does not require pretreatment; (4) MD is not limited by salt concentration, since the water vapor pressure is poorly reduced as the salt concentration increases. This fact allows MD to treat wastewater with high salt content, such as RO brines; (5) it is easy to scale up and (6) the membrane modules offer a large area per unit volume.[14−19]

As discussed, due to its nondependency on the solution concentration, it is quite common to see MD applied, as a further concentration step, in the treatment of RO brines of different nature,[20] deriving from seawater[21] or process wastewaters.[22,23] For what concerns the concentration of sodium sulfate solutions, most of the research is conducted with DCMD or membrane crystallization.[24−27] Sodium sulfate can be present in several process streams, and therefore, it can be in aqueous solution together with other compounds, which affect the efficiency of the separation. It has been observed that sodium-containing solutions behave very similarly (NaCl and Na_2SO_4 in Kurdian et al.,[26] to have a positive solubility-temperature coefficient and a negative solubility-temperature coefficient respectively), and that the lower the ΔT between permeate and retentate, the lower the flux through the membrane, with fluxes in the range 5−25 $kg{\cdot}m^{-2}{\cdot}h^{-1}$. It was also observed in DCMD that the presence of soluble silica within the brine determines a decrease in the flux in two different stages: a first stage with a sudden drop, and a second more gradual decreasing stage.[28] This was elucidated as the deposition of silica onto the membrane, becoming wet out and subsequently depositing gradually at a deeper layer within the membrane.

The DCMD is by far the most consolidated technology, even though it does not have a wide range of applications from a business standpoint, mainly because of the huge energy consumption due to a significant energy loss.[29] The AGMD, on the other hand, is a promising desalinization technology, and can be considered a good compromise between heat loss and transfer resistance.[30] This concept has been theoretically explained[31,32] and extensively studied by Alklaibi and Lior,[33] who evaluated that the process thermal efficiency is 6% higher in AGMD than DCMD, and this gap in further increased by either one between decreasing the inlet temperature and increasing the inlet velocity of the cold stream, which both negatively impact on the DCMD configuration's thermal efficiency. On the other hand, to the best of our knowledge, not much has been investigated in AGMD configuration, especially in the field of Na_2SO_4 brines. Strategies for the enhancement of the flux have been proposed,[34] as well as suggestions like batch recirculation or different concentration stages (continuous operations)[35] to increase the recovery. On a lab scale, flux as high as 25 $kg{\cdot}m^{-2}{\cdot}h^{-1}$ have been reported,[36] even though this result is not fairly comparable to the ones achieved on a larger scale (0.5−4 $kg{\cdot}m^{-2}{\cdot}h^{-1}$).[6,37]

Numerical simulation of MD processes has been approached by many researchers. Nowadays, almost anything requires an accurate mathematical representation, since a trustworthy model can spare much of the expensive and time-consuming job that is evaluating the effect of each operating condition change on the system.[38] Models following the Nusselt number-based approach have been proposed, and a comprehensive review has been recently given by Olatunji and Camacho.[39] These models have important applications from the perspective of using them in industry to predict the behavior of a system when perturbed by an external agent. In addition, however, most of the mathematical models reported in the literature so far aim to calculate specific parameters in a section where they cannot be experimentally measured, giving more details of the operation of the membranes. For instance, the interfacial temperature is a key parameter of the developed models, and it was attempted to be measured experimentally but this approach needs a specifically designed equipment and numerous assumptions.[40]

In northern Spain, Industrias Qumicas del Ebro (IQE) is particularly interested in a technological solution for effective Na_2SO_4 brine treatment in the precipitated silica manufacturing process. In IQE, in the framework of the LIFE ZEROSILIBRINE project, RO concentrates the initial stream up to 12 wt %, and crystallization provides solid sodium sulfate. To improve the efficiency of the process and to comply with the standards of circular economy, the combination of three techniques is now being evaluated: RO + MD + crystallization. The concept is to increase the concentration of the RO product via MD, thus decreasing the energy consumption in the crystallizer. This study investigated the concentration of Na_2SO_4 brine using AGMD technology and developed a mathematical model to verify the consistency of the experimental results and predict the behavior of the system in different operating conditions. Hence, this study provide a full overview, both from an experimental and mathematical point of view, of sodium sulfate brine desalination in AGMD configuration. The experiments have been conducted on a significant scale plant and continuously operating the facility (24/7) for two months, reproducing the operation of an industrial plant, thus making these results particularly significant for the industrial sector.

MATERIALS AND METHODS

AGMD System. To evaluate the system performances, a real brine and a simulated one have been tested with an initial concentration of 120 $g{\cdot}L^{-1}$, which corresponds to the concentration expected at the outlet of the RO process (upstream the membrane) in IQE. The simulated brine was prepared with distilled water and Na_2SO_4 (Los productos de Aldo, Spain), in exact amount to reproduce the desired concentration, while the real brine was provided directly by IQE, with an initial sodium sulfate concentration of 16 $g{\cdot}L^{-1}$, and was concentrated in the laboratory experimental facility up to the expected value for RO retentate prior to further experiments. The experiments were carried out in an AGMD pilot plant provided by Apria Systems. This pilot plant is composed of an MD module integrated in a system with two hydraulically separated circuits, one for the hot brine and one for the cooling solution, which consists of distilled water. It has an 80 L PP feed tank equipped with a 3 kW electric resistance heating system with a feed pump (Figure 1). Cooling is controlled by an external temperature sensor. A centrifugal pump helps to ensure thermal homogeneity by recirculating fluid (chilled water) inside the tank (80 L). The hot and cold streams are fed in a countercurrent flow to the membrane

https://doi.org/10.1021/acs.iecr.3c03415
Ind. Eng. Chem. Res. 2024, 63, 1546−1553

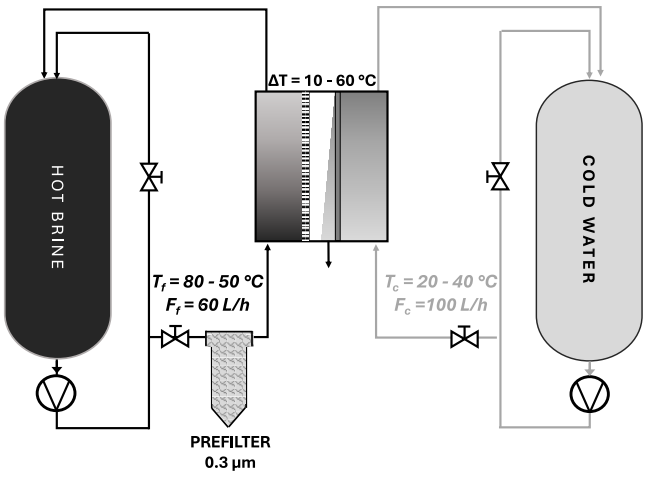

Figure 1. Scheme of AGMD equipment.

module, which houses a membrane area of 250 cm^2 (Sterlitech, poly(tetrafluoroethylene), 45 μm). This is an AGMD module with an airtight air chamber, and the distillate is collected when it condenses on a cold plate. Furthermore, prior to the entry into the membrane module, a prefilter with a pore diameter of 0.3 μm has been installed to capture any potential particles present in the brine. This precautionary measure is particularly crucial in the case of industrial brine solutions. The purpose of this process is to prevent the arrival of substances that could potentially foul or contaminate the membrane. The installation features temperature sensors for both the inlet and outlet of the membrane, as well as pressure sensors. Additionally, there are two rotameters that allow for the establishment and modification of the flow rates of both hot brine and cold water (F_f and F_c, respectively). The flow rate of the distillate was measured gravimetrically. To analyze the evolution of the brine concentration, a conductivity meter (Thermo Fisher Scientific) was employed.

Mathematical Model. The mathematical modeling of MD involves the application of mass and energy balance equations. These equations are used to describe the behavior of the system and predict the real temperatures of the membranes, which, in turn, allow estimation of the actual membrane flux. Vapor transport across the membrane in the AGMD mode is generally described by molecular diffusion theory. Non-condensable gases and the air inside the membrane pores and in the air gap between the membrane and the condensation surface on the permeate side are also described in that model. The model involves solving the mass and energy balances of the process. One-dimensional models have been previously conducted, yielding satisfactory outcomes.[41−43]

Water flux through the membrane and the air-gap (J) can be described, according to Darcy's law, as eq 2, where B_m ($L{\cdot}m^{-2}{\cdot}s^{-1}{\cdot}Pa^{-1}$) is the membrane coefficient—a function of MD configuration, membrane temperature, and membrane characteristics—and Δp represents the pressure difference between the partial pressure of water at the feed membrane surface (P_{mf}) and at the permeate membrane surface (P_p).

$$J = B_m \Delta p = B_m(P_{mf} - P_p) \tag{2}$$

In order to calculate the membrane coefficient, the governing transport phenomena must be assessed among Knudsen, molecular, and viscous flow. The Knudsen number (K_n), is given by eq 3, were k_B is the Boltzmann constant (1.38×10^{-23} $J{\cdot}K^{-1}$), $2r$ is the diameter of the pores of the membrane, which is the characteristic length, and d_{vap} is the water vapor collision diameter.

$$K_n = \frac{\lambda}{2r} = \frac{k_B T}{2r\pi d_{vap}{}^2 P\sqrt{2}} \tag{3}$$

In this case, for a membrane with a pore diameter of 0.45 μm, a pressure of 101 kPa, and temperature in the range 60−80 °C, Knudsen flow, and molecular diffusion govern the transition flow. Thus, the equation to calculate the water flux through the membrane is given as eq 4, where the diffusion coefficient for water/air can be expressed as eq 5.[17]

$$J = \left(\frac{3(\tau\delta + b)}{2r\varepsilon} \cdot \left(\frac{\pi RT}{8M_w} \right)^{0.5} + \frac{(\tau\delta + b)RTP_a}{\varepsilon P_T D_{w/a} M_w} \right)^{-1} \Delta p \tag{4}$$

$$PD_{water/air}\left(\frac{Pa{\cdot}m^2}{s}\right) = 1.895 \times 10^{-5} T^{2.072} \tag{5}$$

In the AGMD process, heat transport takes place through the following phenomena:

- Heat transfer from the brine feed to the membrane surface, expressed as eq 6, where T_f and T_{mf} are the bulk temperature of the feed and the temperature of the feed at the membrane surface respectively, J is the mass flux, $C_{p,f}$ is the specific heat capacity of the feed, and h_f' is the convective heat transfer coefficient. Simplifying the equation, it is possible to define h_f as global heat transfer coefficient in the feed section.
- Heat transfer from the membrane surface, through the pores and the air space, to the condensate (eq 7), which accounts for the sensible heat flux and the vaporization at membrane hot surface. The heat transfer coefficient h is given by eq 8;[42,44] it gives also the effect of finite mass transfer rates on the heat transfer coefficient.[15] C_{cd}, H_v, b, and k_y are respectively the gas (air + vapor) specific heat capacity, the latent heat of vaporization, the air-gap thickness, and the gaseous thermal conductivity.
- Heat transfer through the condensate layer and cooling plate to the coolant liquid, given by eqs 9−11, where h_{cd} and h_p respectively are the convective heat transfer coefficient of the condensate layer and the coolant liquid, while k_{cp} and l are respectively the thermal conductivity and the thickness of the cooling plate.

$$Q_f = h_f'(T_f - T_{mf}) + JC_{p,f}(T_f - T_{mf}) = h_f(T_f - T_{mf}) \tag{6}$$

$$Q_m = h(T_{mf} - T_p) + JH_v \tag{7}$$

$$h = \left(\frac{JC_{cd}}{1 - e^{-bJC_{cd}/k_y}} \right) \tag{8}$$

$$Q_{cd} = h_{cd}(T_p - T_{cpp}) \tag{9}$$

$$Q_{cp} = \frac{k_{cp}}{l}(T_{cpp} - T_{cpc}) \tag{10}$$

$$Q_p = h_p(T_{cpc} - T_c) \tag{11}$$

eqs 9−11 can be easily combined according to eq 12, and a global heat exchange coefficient (h_{cdp}) can be defined as eq 13

https://doi.org/10.1021/acs.iecr.3c03415
Ind. Eng. Chem. Res. 2024, 63, 1546−1553

to express the overall heat transfer (Q_{cdp}) across the condensate layer, the cooling plate and the cooling liquid bulk, as eq 14.

$$Q_{cdp} = h_{cd}(T_p - T_{cpp}) = \frac{k_{cp}}{l}(T_{cpp} - T_{cpc}) = h_p(T_{cpc} - T_c) \quad (12)$$

$$h_{cdp} = \left(\frac{1}{h_{cd}} + \frac{l}{k_{cp}} + \frac{1}{h_p}\right)^{-1} \quad (13)$$

$$Q_{cdp} = h_{cdp}(T_p - T_c) \quad (14)$$

At steady state, the heat transferred from the brine feed (Q_f) is equal to the heat transferred through the membrane, which in turn is equal to the heat transferred through the condensate layer and cooling plate to the coolant liquid. Therefore, given the equality of heat fluxes (eq 15), by combining the equations and rearranging, eqs 16 and 17 can be calculated to express respectively the temperature on the membrane surface (feed side), T_{mf}, and the temperature of the permeate film, T_p.

$$Q_f = Q_m = Q_{cdp} \quad (15)$$

$$T_{mf} = T_f - \left(\frac{\left(\frac{1}{h_f} + \frac{1}{h} + \frac{1}{h_{cdp}}\right)^{-1}}{h_f}\right)\left((T_f - T_c) + \frac{JH_V}{h}\right) \quad (16)$$

$$T_p = T_c + \left(\frac{\left(\frac{1}{h_f} + \frac{1}{h} + \frac{1}{h_{cdp}}\right)^{-1}}{h_{cd}}\right)\left((T_f - T_c) + \frac{JH_V}{h}\right) \quad (17)$$

The modeling process begins by assuming the temperatures of the brine at the membrane surface and the cold side, as well as the brine concentration at the membrane surface and calculating the resulting flux. Heat transfer coefficients are determined through correlations that describe the heat transfer across the membrane. Using these parameters, the temperatures at both sides of the membrane and the brine concentration at the membrane surface can be calculated by using the aforementioned equations.

The mass balance equation takes into account the mass flow rates of the feed, permeate, and retentate considering the concentrations of solutes in each stream. The energy balance equation accounts for the heat transfer between the feed, permeate, and retentate as well as the heat losses to the surroundings. These equations, combined with the heat transfer coefficients, allow for determination of the real temperatures of the system.

The mathematical model was developed using MATLAB, employing a straightforward approach where the equations of mass and energy balance have been solved through an iterative process. The procedure begins with an initial assumption of the temperature at the membrane surface. The water flow is then computed based on this assumption, and subsequently, a revised temperature value is determined considering this water flow. This iterative process continued until convergence is attained. At this point, the model provides a reliable estimation of the real membrane temperatures and, consequently, predicts the actual membrane flux.

It is important to note that the accuracy of the mathematical model depends on the quality of the input data such as heat transfer coefficients, concentration profiles, and membrane properties. Experimental data and correlations are commonly used to validate and refine the model, ensuring its reliability in predicting the performance of the MD systems.

RESULTS AND DISCUSSION

Dependency of the Flux on the Operating Parameters. *Synthetic Brine.* To assess the system performance and membrane efficiency, a series of experiments were conducted using a synthetic brine consisting of water and Na_2SO_4, at a 120 g·L^{-1} concentration. The experiments were designed to investigate the impact of various factors, including different partial pressure gradients, temperature in the cold side (ranging from 20 to 40 °C), temperature in the feed side (ranging from 60 to 80 °C), and varying flow rates.

The obtained results are reported in Figure 3, which shows the permeate flux (J) versus DP_W, i.e., the difference between the partial pressure of water at the feed side of the membrane (P_{mf}) and the partial pressure of water at the permeate side (P_p) (see Figure 2). The permeate flux increased with the brine

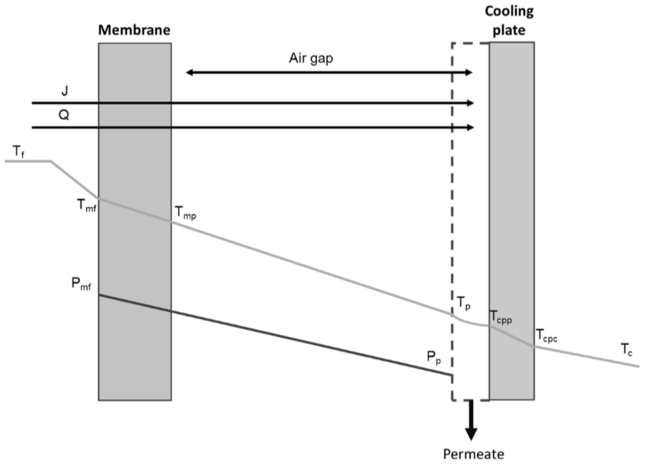

Figure 2. Temperature and pressure profiles for AGMD.

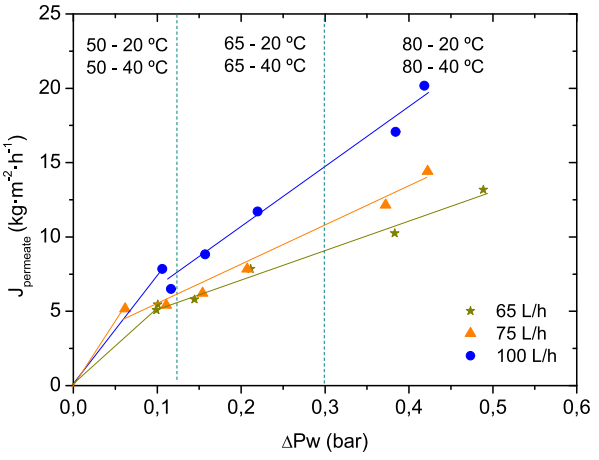

Figure 3. AGMD permeate flux as a function of the driving force, vapor pressure difference (ΔP_w) for the different flow rates.

https://doi.org/10.1021/acs.iecr.3c03415
Ind. Eng. Chem. Res. 2024, 63, 1546−1553

temperature, indicating a direct correlation between the temperature and the rate of permeate production. On the other hand, the AGMD flux displayed limited sensitivity of the coolant temperature. This behavior can be attributed to the minor fluctuations in the partial pressure of water at lower temperatures compared to the ones occurring at the hot side. In the laminar region, it is anticipated that the flux will increase in response to higher feed flow rates, as can be observed from the variation of the flux at the highest ΔP.

Real Brine. In a second set of experiments, the industrial brine was employed in the same conditions to evaluate any possible differences in the behavior compared to the system with synthetic brine. Then, the experiments of Figure 3 where repeated using the real brine. Remarkably, when industrial brine was employed for the tests, it exhibited a trend consistent with that observed with synthetic brine. To perform these tests, the plant processed real brine for a significant time. This means that during the initial operating tests, no signs of membrane deterioration or fouling were detected. Moreover, it is worth noting that the permeate conductivity remained consistently below 20 $\mu S \cdot cm^{-1}$ across all experimental cases, demonstrating the system ability to consistently produce water with excellent purity.

Evolution of Brine Concentration with AGMD System. As stated above, the objective of this work is to concentrate brine using MD technology. In this study, a 120 $g \cdot L^{-1}$ synthetic brine, simulating that obtained from a RO treatment, was utilized. The experiment was conducted under conditions that aimed to maximize the flux, which was achieved—according to the experiments of Section 3.1—by maintaining a high partial pressure difference between the hot side (T_f = 80 °C) and the cold side (T_c = 20 °C). To ensure that the process operated at the desired level, the brine concentration was maintained by removing permeate and replenishing it with an equal amount of brine. A constant brine feed flow rate of 60 $L \cdot h^{-1}$ was maintained during the trials. The flow rate of cold water was 100 $L \cdot h^{-1}$, enough to keep the temperature almost constant in the cold side.

As shown in Figure 4a, the permeate flow rate gradually decreases over the course of the operation days. The reduction in AGMD permeate flux can be linked to the increase in brine concentration. As concentration rises, the water activity decreases, consequently lowering the partial pressure (driving force) for vapor transport.

No concentration polarization is observed as the permeate flow decreases due to a lower driving force resulting from the increased salt concentration. This is attributed to the decrease in water activity associated with higher solute concentration, restricting water molecule movement, and diminishing the driving force for vapor transport. Additionally, the absence of temperature polarization results from the lack of significant temperature gradients across the membrane, as mentioned. Moreover, the obtained water exhibited very low conductivity (less than 20 $\mu S \cdot cm^{-1}$), indicating high rejection values and no fouling phenomena. This outcome demonstrates the applicability of the AGMD technology for the treatment of highly concentrated RO brines.

The evolution of water flux through the membrane, pressure drop in the prefilter, and brine concentration along time are reported in Figure 4. A pressure increase in the feed stream was observed (Figure 4a), due to the fouling of the prefilter (see Figure 1). When working with industrial brine, a prefilter is necessary, and it would be advisible to use two filtration units

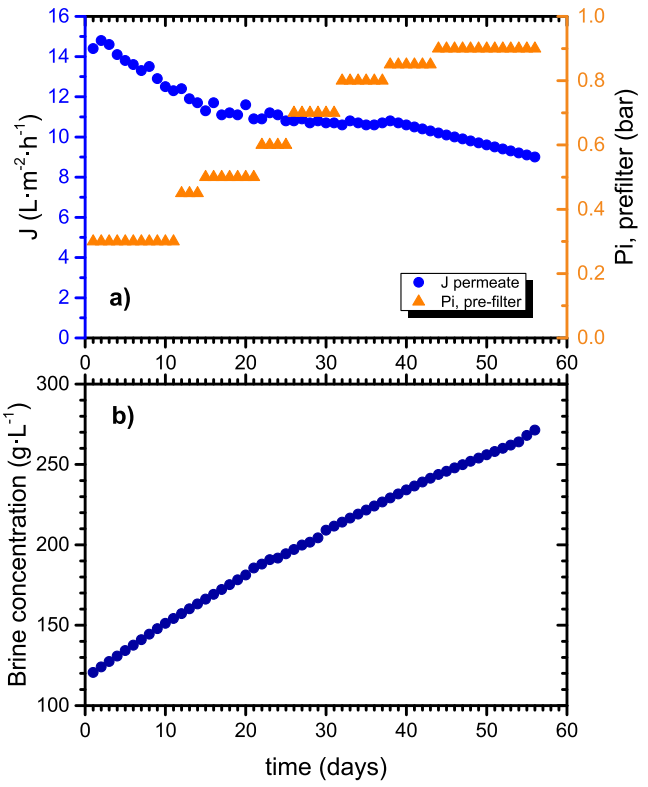

Figure 4. Evolution with the time of the flux (J) (parts a,b) and the concentration of the remaining brine (b). The increase of pressure drop in the prefilter of the feed stream due to fouling is also shown in panel (a) (triangles).

in parallel, to permit cleaning while continuing the operation. This fouling occurs due to retention of particles in the prefilter, although it does not affect the operation of the MD, since the pressure at the hot side of the membrane was always atmospheric pressure. The water flux through the membrane decreased over time (Figure 4a) corresponding to the increase in brine concentration (Figure 4b).

The study aimed to investigate how the permeate flow varies with the temperature and the concentration of the brine itself. The permeate flow is a differentiating factor, as it determines the membrane area used and, consequently, the operational cost of the process. In the experiments conducted to observe the evolution of permeate flow as a function of concentration, special attention was given to the temperature gradient used (i.e., hot side−cold side), which was the highest in the range 80−20 °C.

According to the obtained experimental data, the permeate flow decreased as the brine concentration increased (Figure 5a). This decrease can be primarily attributed to the decrease in the water activity in the solution. As the salt concentration increases, the water activity decreases, resulting in a reduction of the water partial pressure in the solution. This reduction in water partial pressure decreases the driving force for vapor transport through the membrane, leading to a decrease in the permeate flow.[7,45] As per the provided experimental results, the permeate flux started at 14 $L \cdot m^{-2} \cdot h^{-1}$ when the brine concentration was 120 $g \cdot L^{-1}$ and decreased to nearly 9 $L \cdot m^{-2} \cdot h^{-1}$ when the concentration reached 275 $g \cdot L^{-1}$. This represents a reduction in the permeate flow of approximately 35%.

https://doi.org/10.1021/acs.iecr.3c03415
Ind. Eng. Chem. Res. 2024, 63, 1546−1553

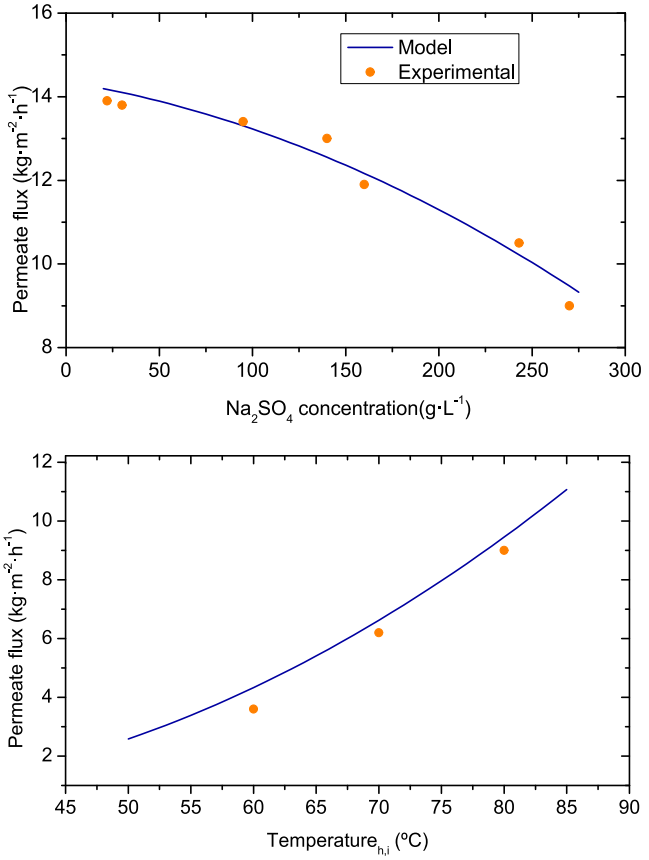

Figure 5. Effect of brine concentration (a) and temperature (b) on permeate flux (J). Symbols represent the experimental data. Continuous curves correspond to the permeate flux predicted by the theoretical model.

Effect of Brine Concentration and Temperature on Permeate Flux. Testing of the Mathematical Model. To observe the effect of temperature, the temperature on the cold side (T_c) was kept fixed at 20 °C, while only the temperature on the hot side (T_f) was varied. As seen in Figure 5a, the flow increased as the temperature in the brine arose. As the temperature increases, the water vapor pressure in the hot side also increases, creating a greater water partial pressure gradient between the feed and the permeate, which promotes a higher permeate flow. These experiments were carried out with the highest brine concentration (280 g·L^{-1}), and the decrease with temperature was quite pronounced, resulting in a flow reduction of 66% for a 20 °C drop in the feed temperature.

Figure 5 also shows that the mathematical model (solid curves) described in previous sections of this paper predicted the experimental data. This correspondence between the model predictions and the experimental results supports its effectiveness as a reliable tool for estimating permeate fluxes in different scenarios. The model ability to capture the effects of key parameters such as brine concentration, temperature, and flow rate demonstrates its utility in the precise prediction of permeate flux under a wide range of conditions.

Ultimately, the effects of different variables on the permeate flow have been examined. In MD is essential to find the optimal balance between using a large temperature difference, to achieve high flow and lower membrane area cost but high-energy consumption, and a smaller temperature difference, that incurs higher membrane costs but lower energy costs. Determining this compromise will depend on the availability of residual or renewable energy and the specific needs of each industry. However, it is clear that the use of modeling and simulation tools can help find this balance and maximize the benefits of MD processes.[46,47]

CONCLUSIONS

An experimental and theoretical study of MD for the treatment of brine from previous RO was carried out. The effect of flow rate, brine and coolant temperature, and brine concentration have been analyzed. MATLAB was used to calculate the permeate flow rate using the mass and energy balances of the process.

Experimentally, it has been found that the permeate flux decreased by 35% when the concentration increased from 120 to 270 g·L^{-1}. However, the decrease is significantly higher when the driving force was lowered by reducing the brine temperature from 80 to 60 °C. In all cases, the salt retention values were above 99%. The model predicts well the flux through the membrane when changing the temperature in the hot and cold sides and the concentration of brine. Taking into account the conditions outlined in this study and the utilization of a real industrial brine, the demonstrated capability of the proposed model to accurately replicate experimental data renders it a powerful tool, especially from an industrial standpoint.

AUTHOR INFORMATION

Corresponding Author

Miguel Menéndez − *Catalysis and Reactor Engineering Group (CREG), Aragón Institute of Engineering Research (I3A), Universidad Zaragoza, 50018 Zaragoza, Spain;* orcid.org/0000-0002-2494-102X; Email: qtmiguel@unizar.es

Authors

Patricia Ugarte − *Catalysis and Reactor Engineering Group (CREG), Aragón Institute of Engineering Research (I3A), Universidad Zaragoza, 50018 Zaragoza, Spain*

Simona Renda − *Catalysis and Reactor Engineering Group (CREG), Aragón Institute of Engineering Research (I3A), Universidad Zaragoza, 50018 Zaragoza, Spain;* orcid.org/0000-0002-5926-5252

Miguel Cano − *Industrias Químicas del Ebro S.A. Grupo IQE, 50016 Zaragoza, Spain*

Jorge Pérez − *Industrias Químicas del Ebro S.A. Grupo IQE, 50016 Zaragoza, Spain*

José Ángel Peña − *Catalysis and Reactor Engineering Group (CREG), Aragón Institute of Engineering Research (I3A), Universidad Zaragoza, 50018 Zaragoza, Spain;* orcid.org/0000-0002-8383-4996

Complete contact information is available at: https://pubs.acs.org/10.1021/acs.iecr.3c03415

Notes

The authors declare no competing financial interest.

ACKNOWLEDGMENTS

Authors acknowledge the support from the Government of Aragón (Spain) through the project "Upgrading of waste water from precipitated silica by circular economy, incorporating the use of the membrane distillation technology" (reference EC-

208-2022 from the call "Supporting industrial research and/or experimental developments in circular economy").

■ ACRONYMS AND SYMBOLS

List of acronyms

AGMD	air-gap membrane distillation
DCMD	direct contact membrane distillation
MD	membrane distillation
RO	reverse osmosis
SGMD	swept gas membrane distillation
VMD	vacuum membrane distillation

List of symbols

$2r$	representative length: membrane pore diameter m
b	air-gap thickness m
B_m	membrane coefficient $kg{\cdot}m^{-2}{\cdot}s^{-1}{\cdot}Pa^{-1}$
C_{cd}	gas specific heat capacity J $(kg{\cdot}K)^{-1}$
$C_{p,f}$	feed specific heat capacity J $(kg{\cdot}K)^{-1}$
d_{vap}	water vapor collision diameter M
$D_{w/a}$	water−air diffusion coefficient $m^2\ s^{-1}$
h	overall heat transfer coefficient in membrane + air gap $W{\cdot}m^{-2}{\cdot}K^{-1}$
h_{cd}	heat transfer coefficient in the condensate film $W{\cdot}m^{-2}{\cdot}K^{-1}$
h_{cdp}	overall heat transfer coefficient in condensate + cooling plate + coolant bulk $W{\cdot}m^{-2}{\cdot}K^{-1}$
h_f	overall heat transfer coefficient in the feed bulk $W{\cdot}m^{-2}{\cdot}K^{-1}$
h_p	heat transfer coefficient in the coolant bulk $W{\cdot}m^{-2}{\cdot}K^{-1}$
H_v	latent heat of vaporization $W{\cdot}m^{-2}$
J	water vapor flux through the membrane $kg{\cdot}m^{-2}{\cdot}s^{-1}$
k_B	Boltzmann constant $J{\cdot}K^{-1}$
k_{cp}	cooling plate thermal conductivity $W{\cdot}m^{-1}{\cdot}K^{-1}$
K_n	Knudsen number
k_y	gas thermal conductivity $W{\cdot}m^{-1}{\cdot}K^{-1}$
l	cooling plate thickness m
M_w	molecular weight $kg{\cdot}mol^{-1}$
P	average pressure in the membrane Pa
P_a	average pressure of air inside the membrane Pa
P_{mf}	partial vapor pressure at the feed membrane surface Pa
P_p	partial vapor pressure at the permeate membrane surface Pa
P_T	total pressure Pa
Q_f	heat flux through the bulk feed $W{\cdot}m^{-2}$
Q_m	heat flux through membrane + air-gap $W{\cdot}m^{-2}$
Q_{cd}	heat flux through the condensate film $W{\cdot}m^{-2}$
Q_{cp}	heat flux through the cold plate $W{\cdot}m^{-2}$
Q_p	heat flux through the coolant bulk $W{\cdot}m^{-2}$
Q_{cdp}	heat flux through the condensate film + cold plate + coolant bulk $W{\cdot}m^{-2}$
R	gas constant $J{\cdot}(mol{\cdot}K)^{-1}$
T	temperature K
T_c	coolant bulk temperature K
T_{cpc}	temperature at the cooling fluid interface K
T_{cpp}	temperature at the cooling plate surface K
T_f	feed temperature K
T_{mf}	feed temperature at membrane surface K
T_p	permeate temperature at the membrane surface K
T_p	temperature at the permeate film K
δ	membrane thickness m
ε	hydrophobic membrane porosity
λ	mean free path m
τ	tortuosity

■ REFERENCES

(1) Abdul Razak, N. A.; Othman, N. H.; Mat Shayuti, M. S.; Jumahat, A.; Sapiai, N.; Lau, W. J. Agricultural and Industrial Waste-Derived Mesoporous Silica Nanoparticles: A Review on Chemical Synthesis Route. *J. Environ. Chem. Eng.* **2022**, *10* (2), 107322.
(2) Drummond, C.; Mccann, R.; Patwardhan, S. V. A Feasibility Study of the Biologically Inspired Green Manufacturing of Precipitated Silica. *Chem. Eng. J.* **2014**, *244*, 483−492.
(3) Kalla, S.; Upadhyaya, S.; Singh, K. Principles and advancements of air gap membrane distillation. *Rev. Chem. Eng.* **2019**, *35* (7), 817−859.
(4) Zhang, Z.; Atia, A. A.; Andrés-Mañas, J. A.; Zaragoza, G.; Fthenakis, V. Comparative Techno-Economic Assessment of Osmotically-Assisted Reverse Osmosis and Batch-Operated Vacuum-Air-Gap Membrane Distillation for High-Salinity Water Desalination. *Desalination* **2022**, *532*, 115737.
(5) Francis, L.; Ahmed, F. E.; Hilal, N. Advances in Membrane Distillation Module Configurations. *Membranes* **2022**, *12* (1), 81.
(6) Schwantes, R.; Bauer, L.; Chavan, K.; Dücker, D.; Felsmann, C.; Pfafferott, J. Air Gap Membrane Distillation for Hypersaline Brine Concentration: Operational Analysis of a Full-Scale Module-New Strategies for Wetting Mitigation. *Desalination* **2018**, *444* (July), 13−25.
(7) Alkhudhiri, A.; Hilal, N. Air Gap Membrane Distillation: A Detailed Study of High Saline Solution. *Desalination* **2017**, *403*, 179−186.
(8) Feng, C.; Khulbe, K. C.; Matsuura, T.; Gopal, R.; Kaur, S.; Ramakrishna, S.; Khayet, M. Production of Drinking Water from Saline Water by Air-Gap Membrane Distillation Using Polyvinylidene Fluoride Nanofiber Membrane. *J. Membr. Sci.* **2008**, *311* (1−2), 1−6.
(9) Anezi, A. A. A.; Sharif, A. O.; Sanduk, M. I.; Khan, A. R. Potential of Membrane Distillation—A Comprehensive Review. *Int. J. Water* **2013**, *7* (4), 317−346.
(10) Skuse, C.; Gallego-schmid, A.; Azapagic, A.; Gorgojo, P. Can Emerging Membrane-Based Desalination Technologies Replace Reverse Osmosis ? *Desalination* **2021**, *500* (November 2020), 114844.
(11) Andrés-Mañas, J. A.; Roca, L.; Ruiz-Aguirre, A.; Acién, F. G.; Gil, J. D.; Zaragoza, G. Application of Solar Energy to Seawater Desalination in a Pilot System Based on Vacuum Multi-Effect Membrane Distillation. *Appl. Energy* **2020**, *258* (October 2019), 114068.
(12) Zhani, K.; Zarzoum, K.; Ben Bacha, H.; Koschikowski, J.; Pfeifle, D. Autonomous Solar Powered Membrane Distillation Systems: State of the Art. *Desalin. Water Treat.* **2016**, *57* (48−49), 23038−23051.
(13) Saffarini, R. B.; Summers, E. K.; Arafat, H. A.; Lienhard V, J. H. Economic Evaluation of Stand-Alone Solar Powered Membrane Distillation Systems. *Desalination* **2012**, *299*, 55−62.
(14) He, K.; Hwang, H. J.; Moon, I. S. Air Gap Membrane Distillation on the Different Types of Membrane. *Korean J. Chem. Eng.* **2011**, *28* (3), 770−777.
(15) Banat, F. A.; Simandl, J. Desalination by Membrane Distillation: A Parametric Study. *Sep. Sci. Technol.* **1998**, *33* (2), 201−226.
(16) Deshmukh, A.; Boo, C.; Karanikola, V.; Lin, S.; Straub, A. P.; Tong, T.; Warsinger, D. M.; Elimelech, M. Membrane Distillation at the Water-Energy Nexus: Limits, Opportunities, and Challenges. *Energy Environ. Sci.* **2018**, *11* (5), 1177−1196.
(17) Khayet, M.; Matsuura, T. *Membrane Distillation Principles and Applications*; Elsevier, 2011.
(18) Zaragoza, G.; Ruiz-Aguirre, A.; Guillén-Burrieza, E. Efficiency in the Use of Solar Thermal Energy of Small Membrane Desalination Systems for Decentralized Water Production. *Appl. Energy* **2014**, *130*, 491−499.
(19) El-Bourawi, M. S.; Ding, Z.; Ma, R.; Khayet, M. A Framework for Better Understanding Membrane Distillation Separation Process. *J. Membr. Sci.* **2006**, *285*, 4−29.

https://doi.org/10.1021/acs.iecr.3c03415
Ind. Eng. Chem. Res. 2024, 63, 1546−1553

(20) Giwa, A.; Dufour, V.; Al Marzooqi, F.; Al Kaabi, M.; Hasan, S. W. Brine Management Methods: Recent Innovations and Current Status. *Desalination* **2017**, *407*, 1−23.
(21) Bindels, M.; Carvalho, J.; Gonzalez, C. B.; Brand, N.; Nelemans, B. Techno-Economic Assessment of Seawater Reverse Osmosis (SWRO) Brine Treatment with Air Gap Membrane Distillation (AGMD). *Desalination* **2020**, *489* (October 2019), 114532.
(22) Woo, Y. C.; Kim, Y.; Shim, W. G.; Tijing, L. D.; Yao, M.; Nghiem, L. D.; Choi, J. S.; Kim, S. H.; Shon, H. K. Graphene/PVDF Flat-Sheet Membrane for the Treatment of RO Brine from Coal Seam Gas Produced Water by Air Gap Membrane Distillation. *J. Membr. Sci.* **2016**, *513*, 74−84.
(23) Duong, H. C.; Chivas, A. R.; Nelemans, B.; Duke, M.; Gray, S.; Cath, T. Y.; Nghiem, L. D. Treatment of RO Brine from CSG Produced Water by Spiral-Wound Air Gap Membrane Distillation—A Pilot Study. *Desalination* **2015**, *366*, 121−129.
(24) Quist-jensen, C. A.; Macedonio, F.; Horbez, D.; Drioli, E. Reclamation of Sodium Sulfate from Industrial Wastewater by Using Membrane Distillation and Membrane Crystallization. *Desalination* **2017**, *401*, 112−119.
(25) Choi, Y.; Naidu, G.; Lee, S.; Vigneswaran, S. Recovery of sodium sulfate from seawater brine using fractional submerged membrane distillation crystallizer. *Chemosphere* **2020**, *238*, 124641.
(26) Kurdian, A. R.; Bahreini, M.; Montazeri, G. H.; Sadeghi, S. Modeling of Direct Contact Membrane Distillation Process: Flux Prediction of Sodium Sulfate and Sodium Chloride Solutions. *Desalination* **2013**, *323*, 75−82.
(27) Tun, C. M.; Fane, A. G.; Matheickal, J. T.; Sheikholeslami, R. Membrane Distillation Crystallization of Concentrated Salts—Flux and Crystal Formation. *J. Membr. Sci.* **2005**, *257*, 144−155.
(28) Gilron, J.; Ladizansky, Y.; Korin, E. Silica Fouling in Direct Contact Membrane Distillation. *Ind. Eng. Chem. Res.* **2013**, *52*, 10521−10529.
(29) Geng, H.; Wu, H.; Li, P.; He, Q. Study on a New Air-Gap Membrane Distillation Module for Desalination. *Desalination* **2014**, *334* (1), 29−38.
(30) Kalla, S.; Upadhyaya, S.; Singh, K. Principles and Advancements of Air Gap Membrane Distillation. *Rev. Chem. Eng.* **2019**, *35* (7), 817−859.
(31) Khayet, M.; Takeshi, M.. *Membrane Distillation: Principles and Applications*; Elsevier, 2011.
(32) Eykens, L.; Reyns, T.; De Sitter, K.; Dotremont, C.; Pinoy, L.; Van der Bruggen, B. How to Select a Membrane Distillation Configuration? Process Conditions and Membrane Influence Unraveled. *Desalination* **2016**, *399*, 105−115.
(33) Alklaibi, A. M.; Lior, N. Comparative Study of Direct-Contact and Air-Gap Membrane Distillation Processes. *Ind. Eng. Chem. Res.* **2007**, *46* (2), 584−590.
(34) Geng, H.; He, Q.; Wu, H.; Li, P.; Zhang, C.; Chang, H. Experimental study of hollow fiber AGMD modules with energy recovery for high saline water desalination. *Desalination* **2014**, *344*, 55−63.
(35) Geng, H.; Wang, J.; Zhang, C.; Li, P.; Chang, H. High Water Recovery of RO Brine Using Multi-Stage Air Gap Membrane Distillation. *Desalination* **2015**, *355*, 178−185.
(36) Singh, D.; Sirkar, K. K. Desalination by Air Gap Membrane Distillation Using a Two Hollow-Fiber-Set Membrane Module. *J. Membr. Sci.* **2012**, *421−422*, 172−179.
(37) Das, R.; Sondhi, K.; Majumdar, S.; Sarkar, S. Development of Hydrophobic Clay-Alumina Based Capillary Membrane for Desalination of Brine by Membrane Distillation. *J. Asian Ceram. Soc.* **2016**, *4* (3), 243−251.
(38) Hitsov, I.; Maere, T.; De Sitter, K.; Dotremont, C.; Nopens, I. Modelling Approaches in Membrane Distillation: A Critical Review. *Separation and Purification Technology*; Elsevier: Amsterdam March 4, 2015; pp 48−64. .
(39) Olatunji, S. O.; Camacho, L. M. Heat and Mass Transport in Modeling Membrane Distillation Configurations: A Review. *Front Energy Res.* **2018**, *6* (December), 1−18.
(40) Ali, A.; Macedonio, F.; Drioli, E.; Aljlil, S.; Alharbi, O. A. Experimental and Theoretical Evaluation of Temperature Polarization Phenomenon in Direct Contact Membrane Distillation. *Chem. Eng. Res. Des.* **2013**, *91* (10), 1966−1977.
(41) Sene M, M. Y. Daily Estimate of Pure Water in a Desalination Unit by Solar Membrane Distillation. *J. Mater. Sci. Eng.* **2015**, *04* (03), 170.
(42) Attia, H.; Osman, M. S.; Johnson, D. J.; Wright, C.; Hilal, N. Modelling of Air Gap Membrane Distillation and Its Application in Heavy Metals Removal. *Desalination* **2017**, *424*, 27−36.
(43) Khayet, M. Membranes and Theoretical Modeling of Membrane Distillation: A Review. *Adv. Colloid Interface Sci.* **2011**, *164*, 56−88.
(44) Alkhudhiri, A.; Darwish, N.; Hilal, N. Treatment of High Salinity Solutions: Application of Air Gap Membrane Distillation. *Desalination* **2012**, *287*, 55−60.
(45) Guendouzi, M. E.; Dinane, A. Determination of Water Activities, Osmotic and Activity Coefficients in Aqueous Solutions Using the Hygrometric Method. *J. Chem. Thermodyn.* **2000**, *32* (3), 297−310.
(46) Hitsov, I.; Maere, T.; De Sitter, K.; Dotremont, C.; Nopens, I. Modelling Approaches in Membrane Distillation: A Critical Review. *Sep. Purif. Technol.* **2015**, *142*, 48−64.
(47) Guillén-Burrieza, E.; Alarcón-Padilla, D. C.; Palenzuela, P.; Zaragoza, G. Techno-Economic Assessment of a Pilot-Scale Plant for Solar Desalination Based on Existing Plate and Frame MD Technology. *Desalination* **2015**, *374*, 70−80.

https://doi.org/10.1021/acs.iecr.3c03415
Ind. Eng. Chem. Res. 2024, 63, 1546−1553